iScience, Volume *25*

Supplemental information

CCL27 is a crucial regulator of immune homeostasis of the skin and mucosal tissues

Micha L. Davila, Ming Xu, Chengyu Huang, Erin R. Gaddes, Levi Winter, Margherita T. Cantorna, Yong Wang, and Na Xiong

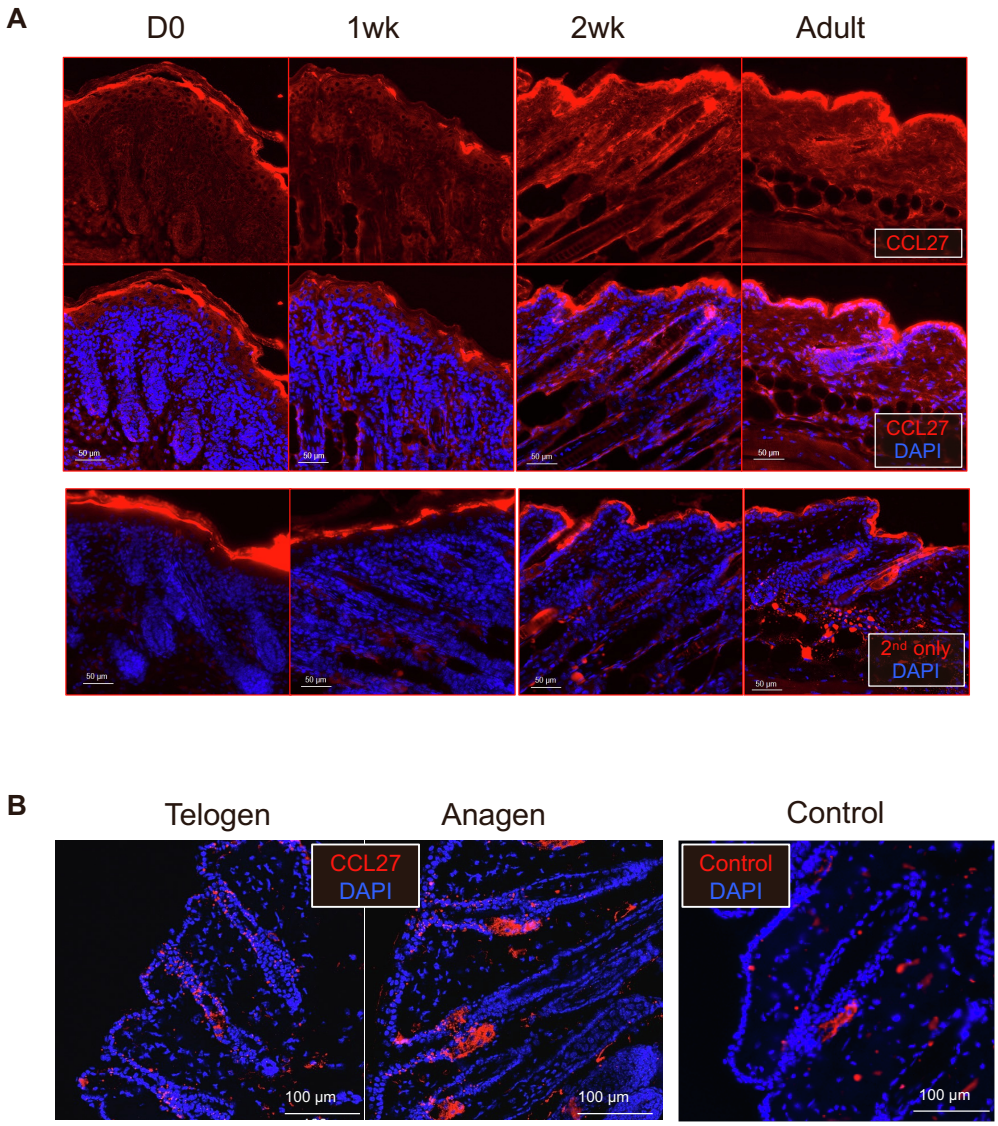

Figure S1. Preferential localization of CCR10^{+} lymphocytes near anagen phase hair follicles correlates with high CCL27 expression by follicular keratinocytes, related to Figure 1. A) Representative immunofluorescent skin sections (14µm) stained with anti-CCL27 antibody. N=7 mice for D0, 1 week, and adult ages and 6 mice for 2 weeks. **B)** Fluorescent images (7µm) representative of skin at resting (telogen) and growing (anagen) phase of hair follicle cycling stained by *in-situ* hybridization with an antisense CCL27 RNA probe or a non-specific RNA probe. The control probe recognizes the DapB gene (accession # EF191515) of a soil bacterial strain Bacillus subtilis SMY. N=3 mice per HF cycle phase. Large red patches are non-specific signals of sebaceous glands that are found in both CCL27 and control probe-stained sections.

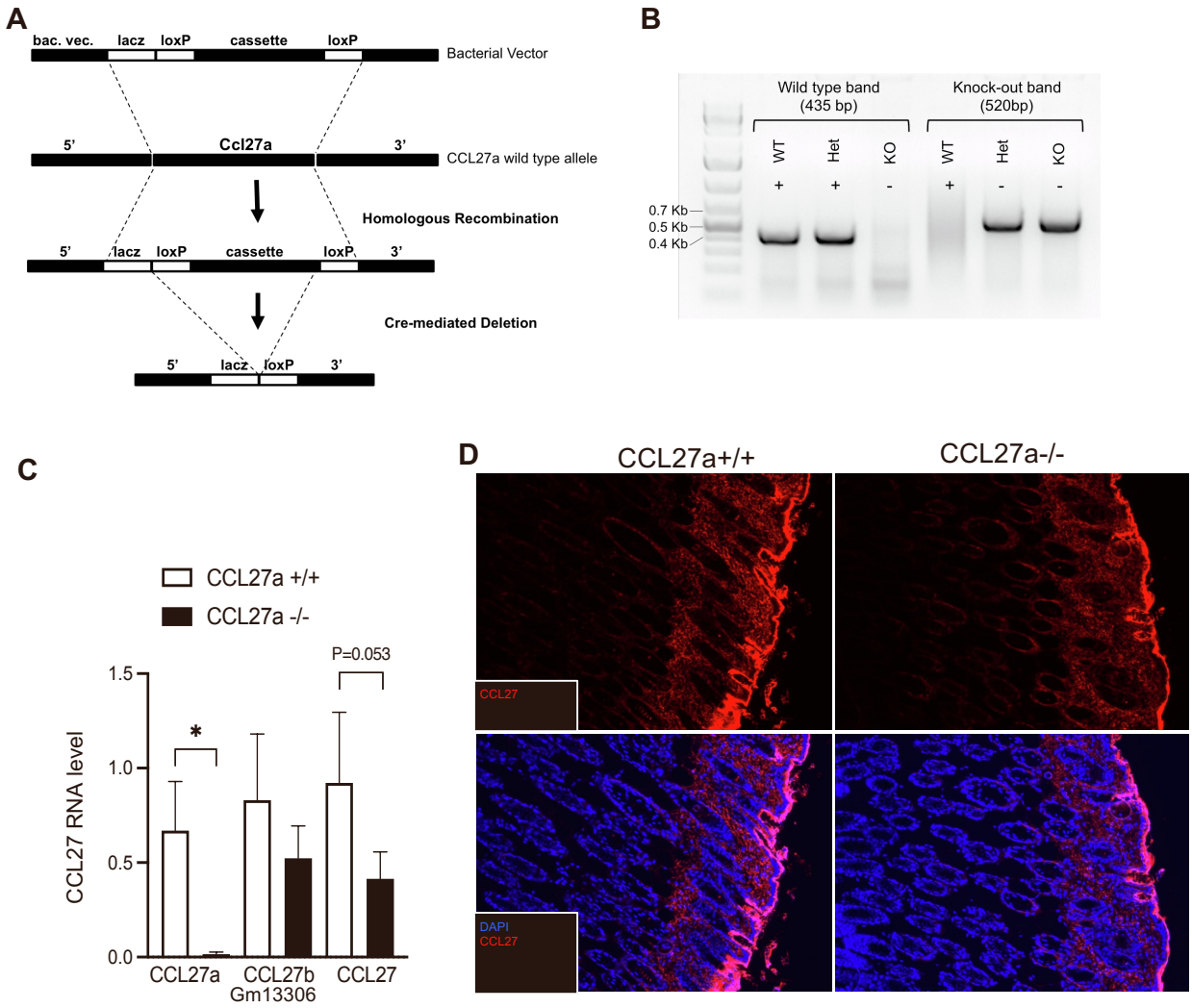

Figure S2. CCL27a-knockout has little effect on the establishment of CCR10^{+} lymphocytes in the skin, related to Figure 2. A) Diagram of the CCL27a-targeting strategy in the CCL27a-knockout mouse line, modified from information obtained from the KOMP Repository (https://www.mmrrc.org/catalog/sds.php?mmrrc_id=46967). **B)** Genomic PCR genotyping CCL27a$^{+/+}$ (WT), heterozygous CCL27a$^{+/-}$ (Het), and homozygous CCL27a$^{-/-}$ knockout (KO) mice. Band sizes of CCL27a-WT and CCL27a-KO alleles are 435bp and 520bp respectively. **C)** Representative immunofluorescent skin sections (15µm) from CCL27a$^{-/-}$ and CCL27a$^{+/+}$ mice stained with anti-CCL27 antibody. **D)** Real-time RT-PCR analysis of total CCL27, CCL27a, and CCL27b/Gm13306 expression in the skin of CCL27a$^{-/-}$ and CCL27a$^{+/+}$ mice. Normalized to β-actin. N=6 mice for each genotype. The predicted coding sequences of CCL27b and Gm13306 are same.

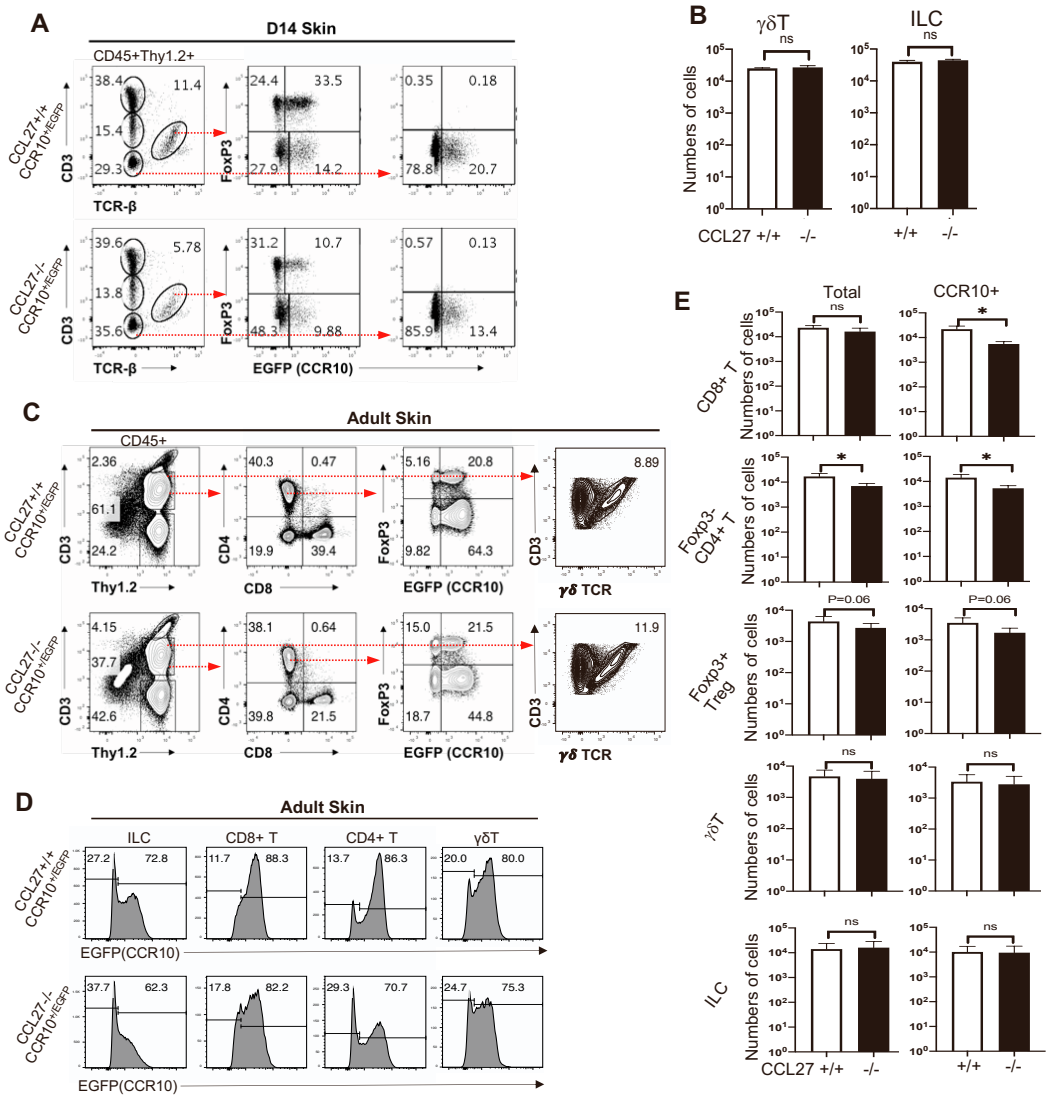

Figure S3. Dysregulated presence of CCR10^{+} lymphocytes in the skin of total CCL27-knockout mice, related to Figure 4. A-B) FC analysis (A) of skin lymphocytes (CD45^{+}Thy1.1^{+}) for numbers of different T cell subsets and ILCs (B) in two week-old CCL27$^{+/+}$CCR10$^{+/EGFP}$ and CCL27$^{-/-}$CCR10$^{+/EGFP}$ mice. αβT cells are CD3^{int+}TCRβ^{+}. Treg cells are CD3^{int+}TCRβ^{+}Foxp3^{+}. ILCs are CD3^{-}TCRβ^{-}. γδT cells are CD3^{int+}TCRβ^{-} (excluding the CD3^{high} dendritic epidermal γδT cells). N=5 for CCL27$^{+/+}$ and 4 for CCL27$^{-/-}$ mice. **C)** FC analysis of skin CD45^{+} immune cells of adult CCL27$^{+/+}$CCR10$^{+/EGFP}$ and CCL27$^{-/-}$CCR10$^{+/EGFP}$ mice for different subsets of T cells and ILCs. **D)** Histograms of CCR10(EGFP) expression in the gated populations of skin T cell subsets and ILCs of adult CCL27$^{+/+}$CCR10$^{+/EGFP}$ and CCL27$^{-/-}$CCR10$^{+/EGFP}$ mice. CD8^{+} and CD4^{+} T cells are gated on CD8^{+} and CD4^{+} CD45^{+}Thy1.2^{+}CD3^{int+}. ILCs are CD45^{+}Th1.2^{+}CD3^{-}. γδT cells are CD45^{+}Thy1.2^{+}CD3^{int+}TCRγδ^{+} (excluding CD3^{high} dendritic epidermal γδT cells). **E)** Numbers of of total and CCR10^{+} CD8^{+}, Foxp3^{-}CD4^{+}, Foxp3^{+}Treg, γδ T cells and ILCs in adult CCL27$^{+/+}$CCR10$^{+/EGFP}$ and CCL27$^{-/-}$CCR10$^{+/EGFP}$ mice. N=11 samples each for total CD8^{+} T cells, 5 each for CCR10^{+} CD8^{+} T cells, 5 each for Foxp3^{-}CD4^{+} and Foxp3^{+}Treg cells, and 4 each for γδT cells and ILCs.

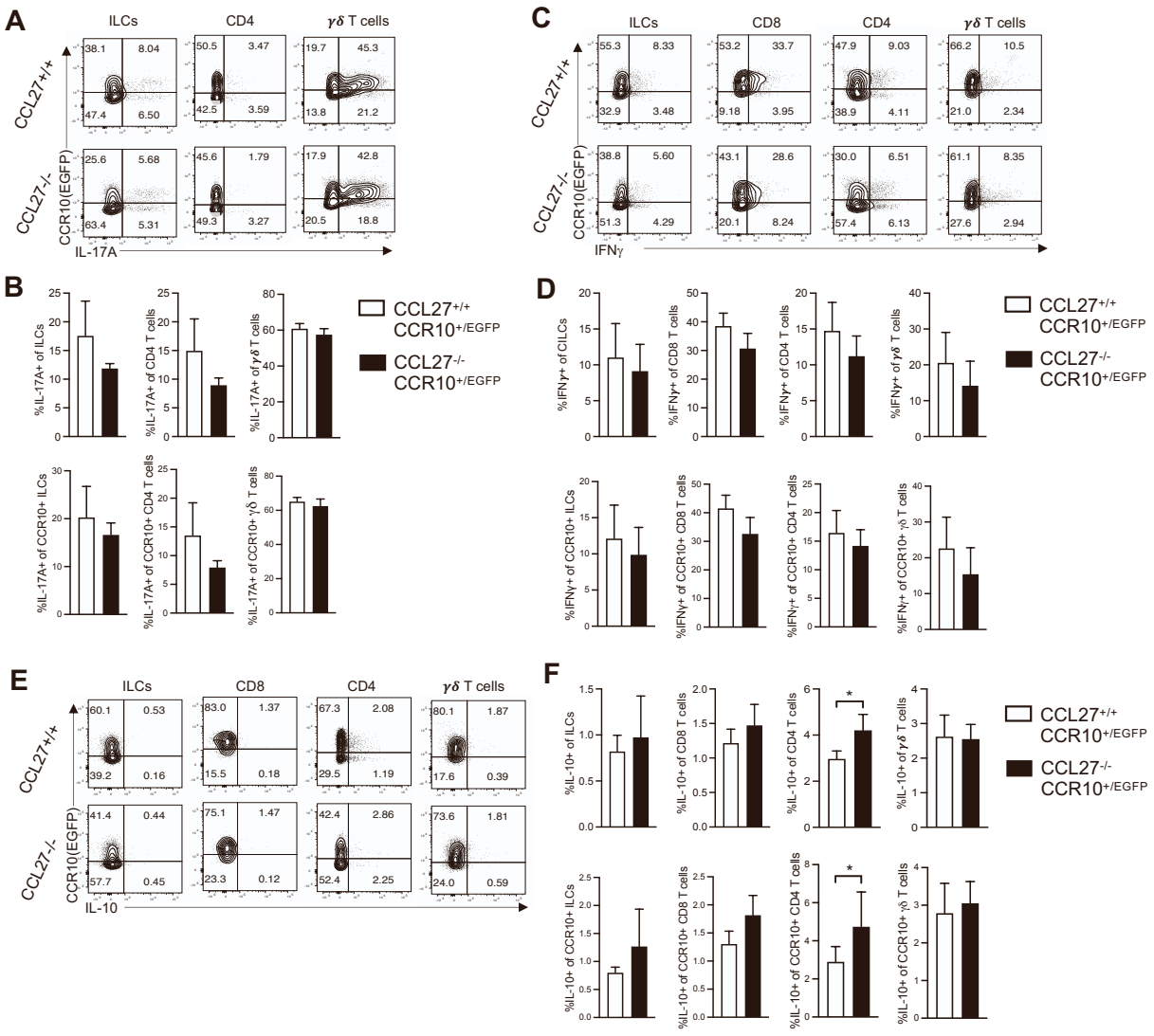

Figure S4. Minor shifts in the cytokine production capacity of skin lymphocytes in CCL27$^{-/-}$ versus WT mice at steady state, related to Figure 4. A-B) FC analysis (A) and graphed percentages (B) of IL-17A production of stimulated skin lymphocytes from adult CCL27$^{+/+}$CCR10$^{+/EGFP}$ and CCL27$^{-/-}$CCR10$^{+/EGFP}$ mice. N=7 mice for each genotype. **C-D)** FC analysis (C) and graphed percentages (D) of IFNγ production of stimulated skin lymphocytes from adult CCL27$^{+/+}$CCR10$^{+/EGFP}$ and CCL27$^{-/-}$CCR10$^{+/EGFP}$ mice. N=6 mice each. **E-F)** FC analysis (E) and graphed percentages (F) of IL-10 production of stimulated skin lymphocytes from adult CCL27$^{+/+}$CCR10$^{+/EGFP}$ and CCL27$^{-/-}$CCR10$^{+/EGFP}$ mice. T cell populations are gated on CD45^{+}CD3^{int+} CD8^{+}, CD4^{+} or γδ TCR^{+}. ILCs are gated on CD45^{+}Thy1.2^{+}CD3^{-}. N=5 mice for each genotype.

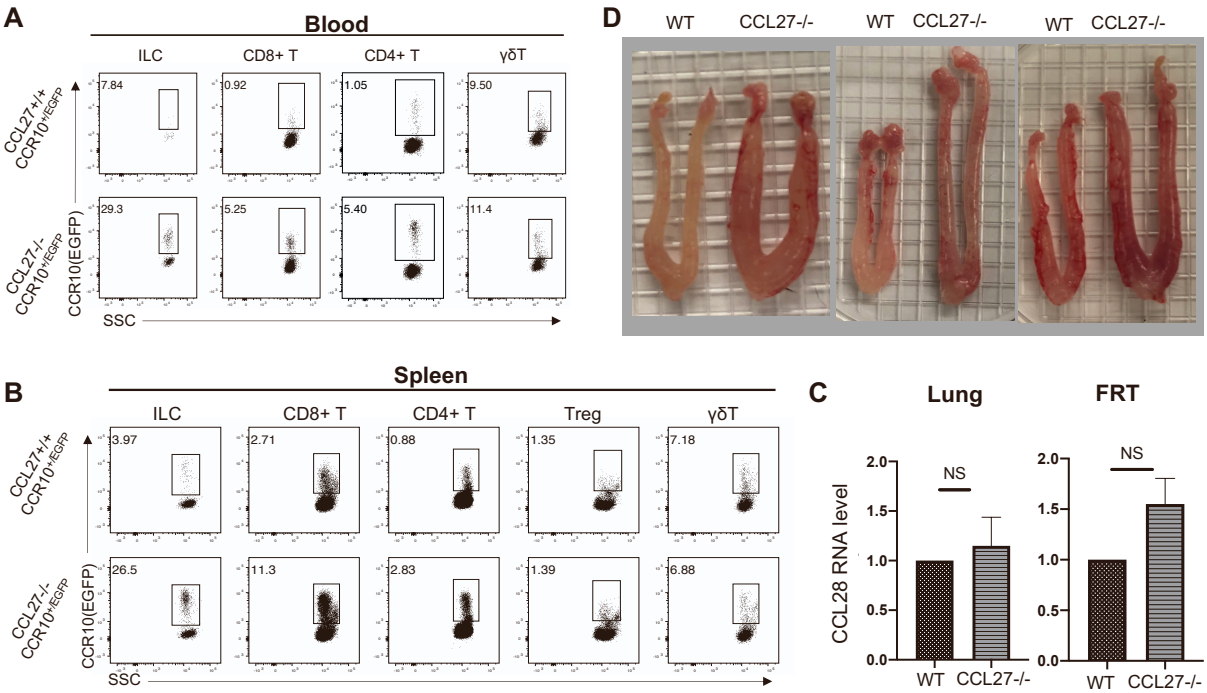

Figure S5. Increased accumulation of CCR10^{+} lymphocytes in the blood, spleens and lungs and female reproductive tracts of total CCL27-knockout mice, related to Figure 6. A-B) FC analysis gating on populations of T cell subsets and ILCs for their CCR10(EGFP) expression in the spleen (A) and blood (B) of adult CCL27$^{+/+}$CCR10$^{+/EGFP}$ and CCL27$^{-/-}$CCR10$^{+/EGFP}$ mice. **C)** Real-time RT-PCR analysis of relative CCL28 expression in lungs and female reproductive tracts (FRT) of CCL27$^{-/-}$ mice in comparison to WT controls. Normalized to β-actin. N=4 each for lungs and 3 each for FRT. **D)** Images of uteri of three pairs of WT and CCL27$^{-/-}$ female littermate mice.